crystals

MDPI

Article

Characterization of Biominerals in Cacteae Species by FTIR

Alejandro De la Rosa-Tilapa [1], Agustín Maceda [2] and Teresa Terrazas [1,*]

[1] Instituto de Biología, Universidad Nacional Autónoma de México, México City 04510, Mexico; aledrosa17@gmail.com
[2] Programa de Botánica, Colegio de Postgraduados en Ciencias Agrícolas, Texcoco, Estado de México 56230, Mexico; biologoagustin@hotmail.com
* Correspondence: tterrazas@ib.unam.mx

Received: 7 May 2020; Accepted: 27 May 2020; Published: 29 May 2020

Abstract: A biomineral is a crystalline or amorphous mineral product of the biochemical activity of an organism and the local accumulation of elements available in the environment. The cactus family has been characterized by accumulating calcium oxalates, although other biominerals have been detected. Five species of Cacteae were studied to find biominerals. For this, anatomical sections and Fourier transform infrared, field emission scanning electron microscopy and energy dispersive X-ray spectrometry analyses were used. In the studied regions of the five species, they presented prismatic or spherulite dihydrate calcium oxalate crystals, as the predominant biomineral. Anatomical sections of *Astrophytum asterias* showed prismatic crystals and *Echinocactus texensis* amorphous silica bodies in the hypodermis. New findings were for *Ariocarpus retusus* subsp. *trigonus* peaks assigned to calcium carbonate and for *Mammillaria sphaerica* peaks belonging to silicates.

Keywords: anatomy; Cactaceae; calcium carbonate; oxalate; silica; stem; weddellite

1. Introduction

A biomineral is a crystalline or amorphous mineral product of the biochemical activity of an organism and the local accumulation of elements available in the environment [1]. In plants, the most common biominerals are amorphous silica, calcium oxalate and calcium carbonate salts [2–7]. Some species of the Cactaceae family accumulate up to 85% of their dry weight in calcium oxalate crystals [8,9]. These calcium oxalate crystals may have one of two states of hydration: monohydrate ($CaC_2O_4 \cdot H_2O$; whewellite) or dihydrate ($CaC_2O_4 \cdot 2H_2O$; weddellite) [10–17]. In addition, other biominerals, such as magnesium oxalate ($MgC_2O_4 \cdot 2H_2O$; Glushinkite) [17], amorphous silica bodies ($SiO_2 \cdot nH_2O$; opal) [18] and silica in crystalline form (SiO_2; α-quartz) [19], have been identified in cacti.

Like other plants, biominerals in Cactaceae develop mainly in the cellular vacuole of different epidermal, fundamental or vascular stem tissues. The accumulation of biominerals in a given tissue is usually highly specific in some species or genera [10,18,20–23]. Thirty-four species from the Cacteae tribe have been studied with techniques such as X-ray diffraction to detect calcium oxalates [11], by Raman spectroscopy in *Ferocactus latispinus* and *Coryphantha clavata* [24] and by Fourier transform infrared (FTIR) only in one species, *Mammillaria uncinata* [25]. In these techniques, the tissues were blended or macerated together, so they have not been analyzed individually in the Cacteae species.

For this reason, the FTIR technique can be a good option to study biominerals due to the minimum amount of sample and the speed of data acquisition. Therefore, the aims of this study were to characterize the biominerals and determine their hydration state in the different tissues of five Cacteae species. With this, it will be possible to identify other biominerals that are not calcium oxalate,

magnesium oxalate or amorphous silica, in addition to the state of hydration of biominerals in the different tissues.

2. Material and Methods

Two adult and healthy plants of five species classified within the Cacteae tribe were collected in their natural habitats (Table 1). For each species, a portion of the plant was prepared as a voucher, which was deposited in the National Herbarium (MEXU). In one of the two plants per species, spines were removed. Then, using a dissecting microscope at different magnifications, the stem of each sample was dissected into the epidermis plus hypodermis (EH), cortex (C), vascular cylinder (VC) and pith (P) (Figure 1A,B). Each tissue was blended with distilled water and filtered with a mesh of approximately 300 µm pore diameter to separate biominerals from cell debris. The biominerals were precipitated, washed with distilled water several times until no residue was observed under a stereomicroscope, and finally, dried at room temperature. Small samples from pith to epidermis were prepared for FE-SEM-EDS (see 2.3, JEOL Ltd., Akishima, Tokyo, Japan).

Table 1. Species analyzed and the state of Mexico where they were collected. Vouchers deposited at MEXU.

Species	Collection Number	Location
Astrophytum asterias (Zucc.) Lem.	TT1020	La Esperanza, Tamaulipas
	TT846	San Carlos Tamaulipas
Ariocarpus retusus subsp. *trigonus* (F.A.C.Weber) E.F.Anderson & W.A.Fitz Maur.	TT1005	La Soledad, Tamaulipas
	TT879	Moctezuma, San Luis Potosí
Echinocactus texensis Hopffer	TT1021	La Esperanza, Tamaulipas
	TT851	Tula, Tamaulipas
Mammillaria melanocentra subsp. *rubrograndis* (Repp. & A.B. Lau) D.R. Hunt	TT1050	Ejido Huizache, Tamaulipas
Mammillaria sphaerica A. Dietr.	TT1051	Ejido Huizache, Tamaulipas

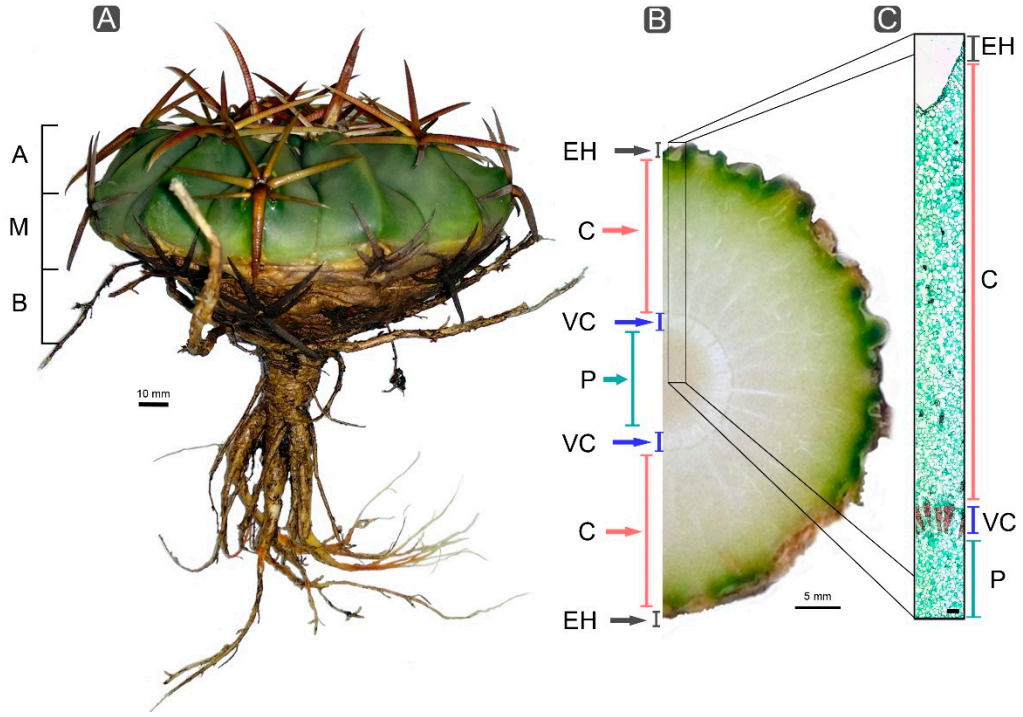

Figure 1. Stem and macro and microscopic tissues studied. (**A**) *Echinocactus texensis* (TT1021), showing the globose depressed stem. (**B**) *Echinocactus texensis*, transverse section illustrating the stem tissues. (**C**) *Mammillaria sphaerica* (TT1051), microscopic transverse section showing the tissues. A = apical, M = medium, B= basal, EH = epidermis-hypodermis, C = cortex, VC = vascular cylinder, P = pith. Bar is 300 µm in C.

The second individual of each species was divided into three parts (apical, median and basal) no larger than 1.5 cm length that included epidermal, cortical, vascular and pith tissues (Figure 1A,C). Each part was immediately fixed in a formalin-acetic acid-ethanol solution (10:5:85) [26] and processed for paraffin embedding according to Loza-Cornejo and Terrazas [27]. Transverse and tangential sections 14 μm thick were made with a rotary microtome, stained with Safranin-fast green, and mounted with synthetic resin.

2.1. Fourier Transform Infrared (FTIR) Spectroscopy Analysis

Approximately 0.1 g of biomineral dry sample of each species was used to obtain the infrared spectra. The spectra were obtained with an Attenuated Total Reflectance Fourier Transform Infrared Spectrometer (ATR-FTIR) (Agilent Cary 630 FTIR, Agilent Technologies, Santa Clara, CA, USA) equipped with an ATR diamond unit [28]. The samples were processed with two wavenumber ranges of 4000–400 cm^{-1} and 4000–650 cm^{-1} (30 scans with a resolution of 4 cm^{-1}, 15 seconds per sample and three replicates per sample) with the program MicroLab PC (Agilent Technologies, Santa Clara, CA, USA). The baseline correction, ATR correction (applied only in 4000 to 400 cm^{-1}) and the spectra average were performed with the Resolution Pro FTIR Software program (Agilent Technologies, Santa Clara, CA, USA). With the spectra obtained, the peaks corresponding to the mineral components were identified and compared with those reported in the literature [29,30].

2.2. Polarized and Brightfield Microscope Analysis

For each species, permanent slides were observed with both types of lighting in an Olympus BX 51 microscope (Olympus, Tokyo, Japan) and photographs obtained with Image Pro Plus 7.1 software (Media Cybernetics, MD, USA) to characterize the morphology and distribution of biominerals in the different tissues of the three regions studied (Figure 1). Additionally, photographs of isolated biominerals from each tissue were also obtained with the two types of lighting.

2.3. Field Emission Scanning Electron Microscopy (FE-SEM) and Energy Dispersive X-ray Spectrometry (EDS) Analysis

For FE-SEM observations, samples from pith to epidermis of stems (<1 cm) per species were placed between to coverslips and dried in an oven (56 °C) overnight. The dried samples were fixed to aluminum specimen holders with double-sided tape and coated with gold in a Hitachi-S-2460N sputter coater. The coated samples were then observed using a Field Emission Scanning Electron Microscope (FE-SEM; JEOL-JSM7800, JEOL Ltd., Akishima, Tokyo, Japan) (20 Kv) coupled to Energy Dispersive X-ray Spectrometry (EDS; Oxford X-Maxn^2 50 mm^2, Oxford Instruments, Tubney Woods, Abingdon, UK) at the Physics Institute, UNAM. It was calibrated with copper and standards were: C (Cvit), O (SiO_2), Mg (MgO), Al (Al_2O_3), Si (SiO_2), K (KBr) and Ca (Wollastonite). The relative concentration of the element is given in percentages of weight.

3. Results

3.1. Analysis by FTIR

Figure 2 shows the spectra of the four tissues analyzed from the five species. In all spectra, the characteristic calcium oxalate crystals peaks were present (Table S1) in all species and in the four tissues. Furthermore, in all the tissues of the five species, a weak peak at 915 cm^{-1} and a wide peak ranging from 3000 to 3600 cm^{-1} due to the OH stretching were present and reflected the occurrence of dihydrate calcium oxalate ($CaC_2O_4{\cdot}2H_2O$). This dihydrate calcium oxalate was detected in *Astrophytum asterias*, *Echinocactus texensis* and *Mammillaria sphaerica* with the peak 517 cm^{-1} (Figure 2A,E,I), although there is noise on the spectra. The peaks between 1014 and 1048 cm^{-1} in some tissues of the five species studied were assigned to opal and silicates (Figure 2B,D,F,H,J), whereas some peaks in the pith of *Ariocarpus retusus* subsp. *trigonus* were assigned to calcium carbonate (Figure 2C,D).

The peaks at 555 and 560 cm^{-1} could represent some contaminants or unknown biomineral residue (Figure 2A–J). The occurrence of primary cell wall debris was assigned to hemicellulose residues in the pith (4) of *Ariocarpus retusus* subsp. *trigonus* (Figure 2D) and to cellulose residues in the pith (4) and epidermis-hypodermis (1) of *Astrophytum asterias* (Figure 2A,B), *Ariocarpus retusus* subsp. *trigonus* (Figure 2C,D) and *Mammillaria sphaerica* (Figure 2I,J).

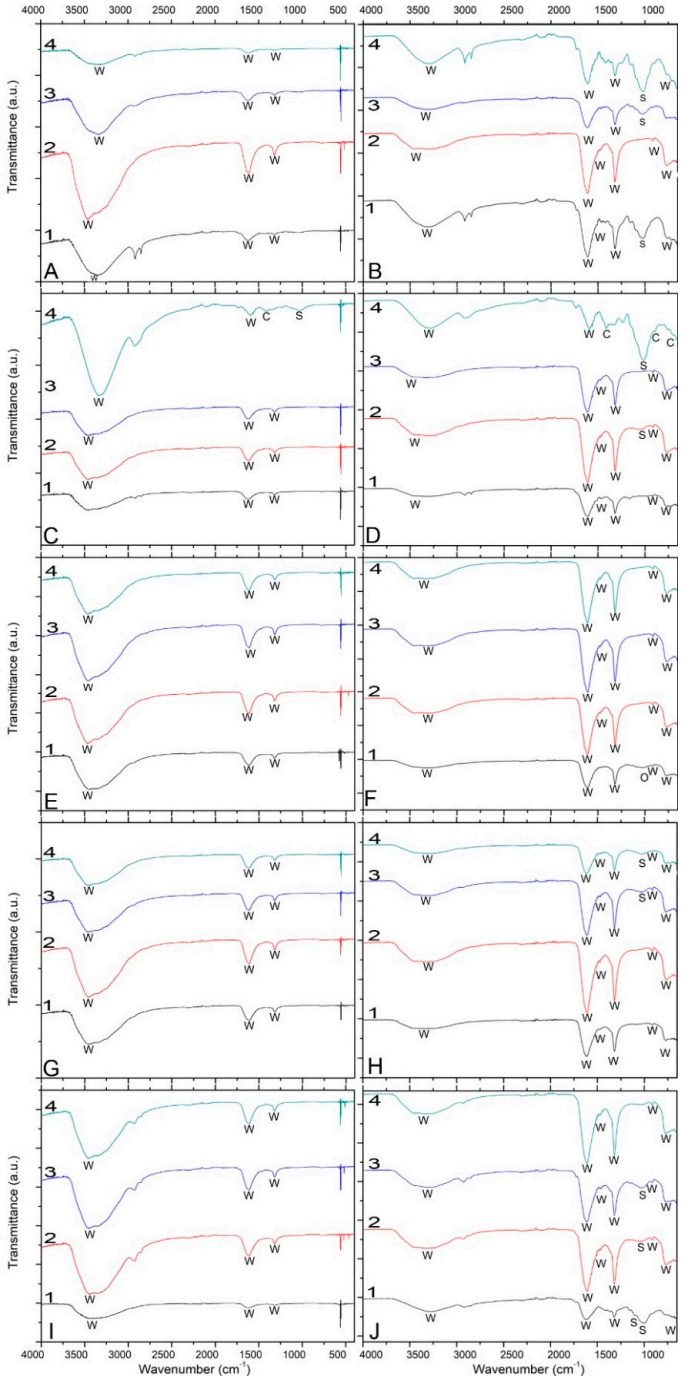

Figure 2. Spectra of biominerals in each tissue studied. The numbers below each spectra (line) indicate the wavenumbers of the peaks. A, C, E, G, I 4000–400 cm^{-1} spectra. B, D, F, H, J 4000–650 cm^{-1} spectra. (**A**,**B**) *Astrophytum asterias*. (**C**,**D**) *Ariocarpus retusus* subsp. *trigonus*. (**E**,**F**) *Echinocactus texensis*. (**G**,**H**) *Mammillaria melanocentra* subsp. *rubrograndis*. (**I**,**J**) *Mammillaria sphaerica*. Tissues: 1(black line) = Epidermis-hypodermis, 2(red) = Cortex, 3(purple) = Vascular cylinder, 4(green) = Pith, W = weddellite (calcium oxalate dihydrate), O = opal (amorphous silica), C = Calcium carbonate, S = silicates.

3.2. Anatomy with Light and Polarized Microscopy

The five species studied have the typical stem anatomy for the Cacteae. There is an epidermis with straight or convex outer cell wall and a hypodermis of one to five strata of parenchyma or collenchyma (Figure 3A,E and Figure 4A). Both cortex and pith have exclusively parenchyma cells (Figure 4A) and in the vascular cylinder, nonfibrous wood with wide medullary unlignified rays (Figure 4F–H). The studied species do not form visible biominerals in the epidermis (Figure 3). Two of the five species studied here had biominerals in the hypodermal cells. *Astrophytum asterias* presented prismatic biominerals (Figure 3A,C) that were birefringent under polarized light (Figure 3B,D) and *Echinocactus texensis* had amorphous silica bodies that lacked birefringence under polarized light (Figure 3E,F). Biominerals in the hypodermal cells of *Ariocarpus retusus* subsp. *trigonus* and both *Mammillaria* species were not detected in the anatomical sections.

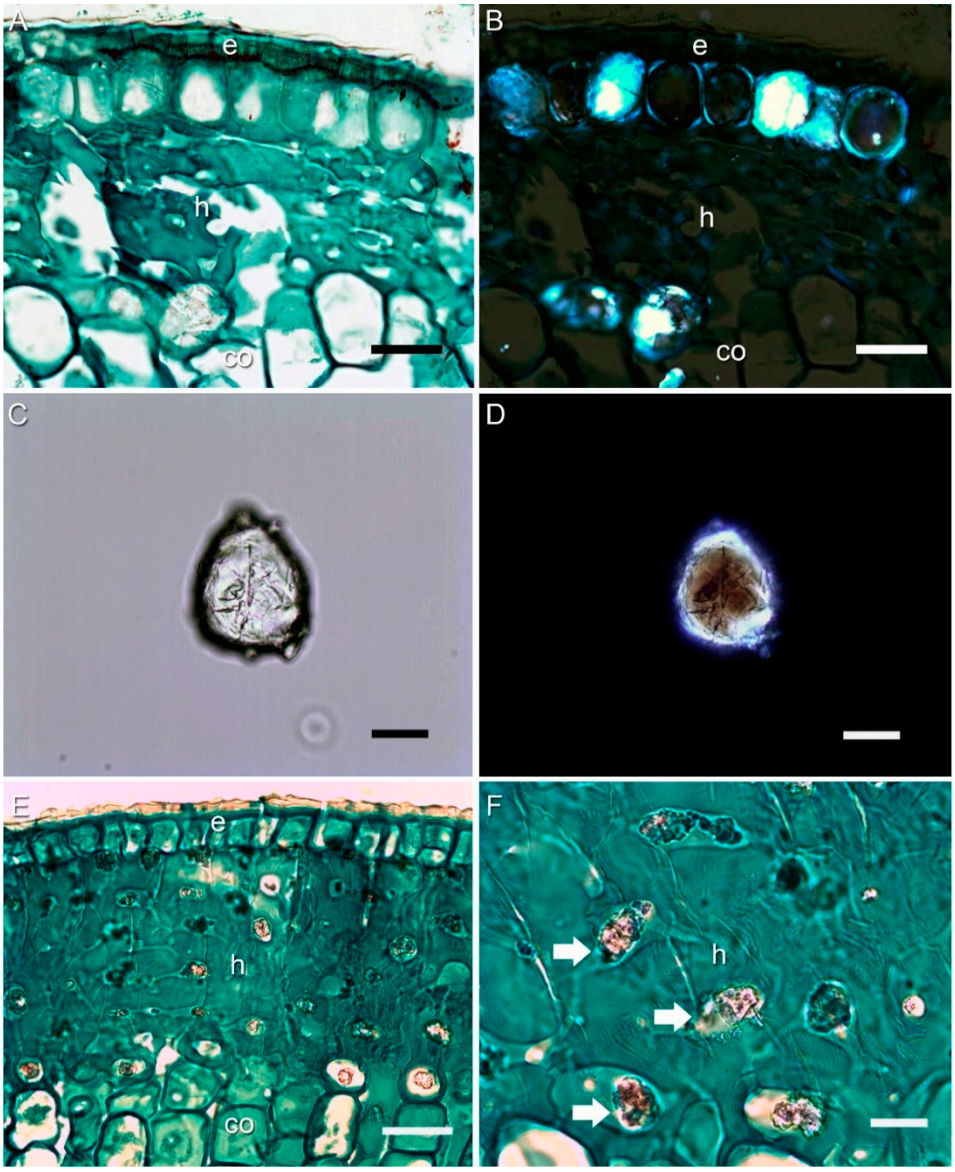

Figure 3. Biominerals in the hypodermis of stem in Cacteae, transverse sections (TS) and isolated (IS). (A, C, D, E, F) Bright field. (B, D) Polarized light. (**A**,**B**) *Astrophytum asterias* (TT846), TS. (**C**,**D**) *Astrophytum asterias* (TT1020), IS. (**E**,**F**) *Echinocactus texensis* (TT859), TS. Bar is 50 µm in A, B, E; 20 µm in C, D, F. e = epidermis, co = cortex, h = hypodermis, white arrows = amorphous silica bodies.

In the cortex (Figure 4A,B,D), vascular cylinder (Figure 4F–H) and pith (Figure 4I,J), all species had spherulites or prisms, which were birefringent with polarized light (Figure 4C,E,G,L,N,P). In the vascular tissue, the biominerals were deposited in the ray cells (Figure 4F,H).

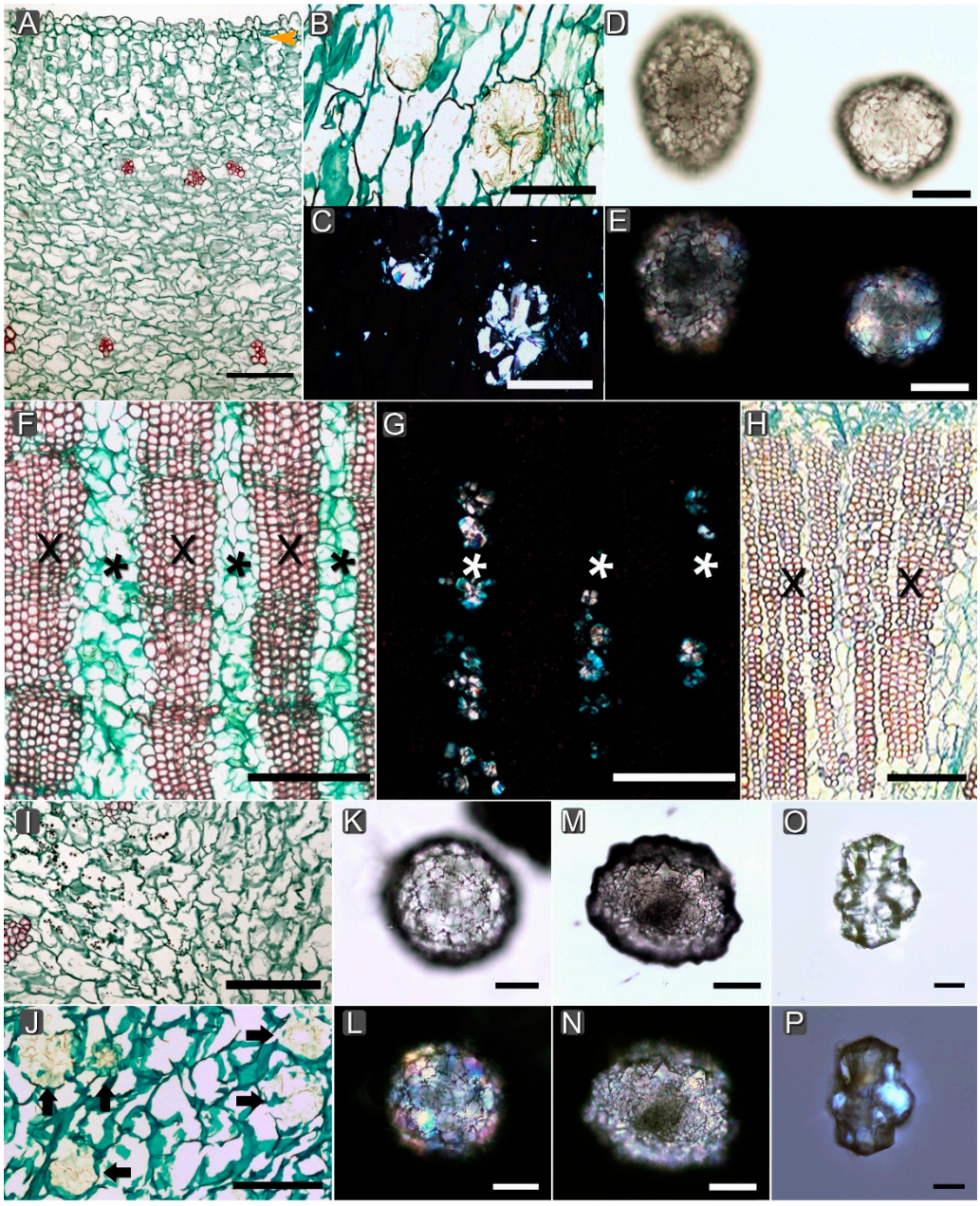

Figure 4. Biominerals in the stem tissues of transverse sections (TS) and isolated (IS) using bright field (b) or polarized light (p). (**A**) *Ariocarpus retusus* subsp. *trigonus* (TT1005), TSbAR, epidermis, hypodermis (orange arrowhead) and cortical tissue. (**B**,**C**) *Astrophytum asterias* (TT846), TSbpMR, spherulites in cortical cells. (**D**,**E**) *Astrophytum asterias* (TT1020), IS, spherulites of cortical tissue. (**F**,**G**) *Echinocactus texensis* (TT859), TSbpBR, spherulites in vascular cylinder. (**H**) *Mammillaria sphaerica* (TT1051), TSbBR, vascular cylinder. (**I**) *Ariocarpus retusus* subsp. *trigonus* (TT879), TSbAR, pith. (**J**) *Echinocactus texensis* (TT859), TSbBR, spherulites (black arrows) in pith. (**K**,**L**) *Ariocarpus retusus* subsp. *trigonus* (TT1005), ISbp, spherulites of cortical tissue. (**M**,**N**) *Mammillaria melanocentra* subsp. *rubrograndis* (TT1050), ISbp, spherulites of pith. (**O**,**P**) *Mammillaria sphaerica* (TT1051), ISbp, spherulites of cortical tissue. Bar is 300 µm in A, B, C, F–J; 100 µm in M, N; 50 µm in D, E, K, L; 20 µm in O, P. AR = apical region; MR = medium region; BR = basal region; X = tracheary cells; * = rays.

3.3. FE-SEM-EDS Analysis

Figure 5 shows the morphology and elements detected by EDS analysis. Differences between hypodermal and cortical element concentrations were observed. *Astrophytum asterias* has the highest concentration Ca (49.53%) and Al (0.87%) in the prismatic crystals of the hypodermis, whereas in *Echinocactus texensis*, hypodermis showed the lowest concentrations of Ca (5.08%) and Al (0.15%), but the highest of Si (25.34%). No traces of Mg, K and Si were detected in *Astrophytum asterias* spherulites (Figure 5F), but traces of Si (0.91), K (0.79%), Mg (0.17%) were detected in *Ariocarpus retusus* subsp. *trigonus* (Figure 5H).

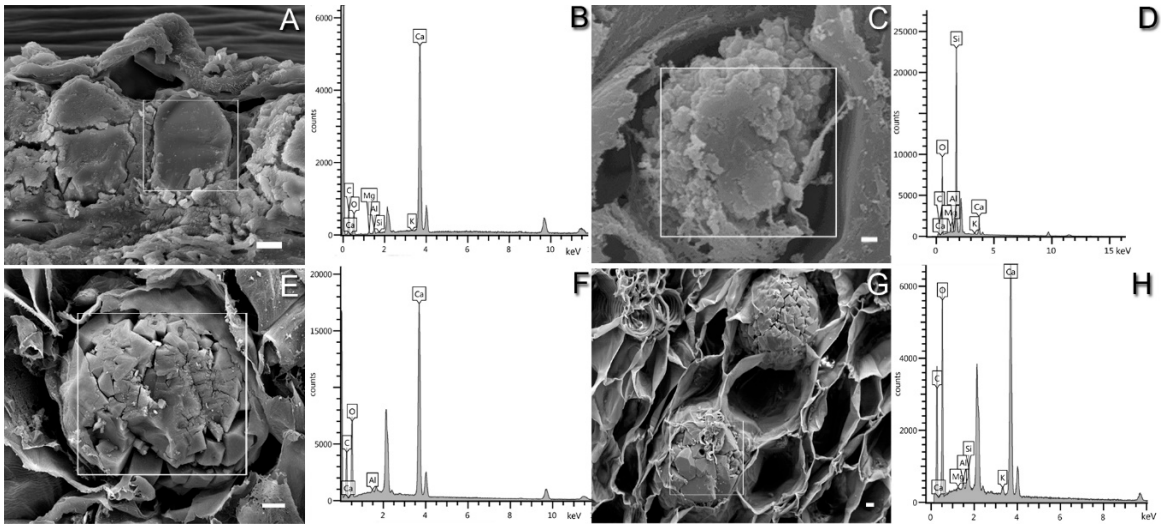

Figure 5. SEM images and EDS spectra for stem tissues of Cacteae species. (**A**,**B**) *Astrophytum asterias* (TT1020), prisms in hypodermis. (**C**,**D**) *Echinocactus texensis* (TT1021), amorphous silica bodies in hypodermis. (**E**,**F**) *Astrophytum asterias*, spherulite in cortex. (**G**,**H**) *Ariocarpus retusus* subsp. *trigonus* (TT1005), spherulites in cortex. The white square on images was the area used to analyze the elements. Bar is 10 µm in A, E, G; 1 µm in C.

4. Discussion

Calcium oxalates and amorphous silica bodies turned out to be the main biominerals in the Cacteae species studied. Both are not exclusive to the cactus family, as calcium oxalates have been described in at least 215 plant families [6] and amorphous silica bodies in 56 [31]. However, the presence of these biominerals in Cactaceae has had great relevance in its systematics, because they are not deposited randomly in the stem tissues [20,23]. Moreover, it has been suggested the possibility of identifying biominerals other than calcium oxalate [10,21,23] and different crystalline structures have been described even within the stem of the same species [23] as we found in the studied species. Calcium carbonate is poorly described for Cactaceae, possibly due to the fixation technique of the samples, so that unfixed samples combined with the FTIR analysis favor the recognition of calcium carbonate as well as the presence of other compounds.

4.1. Biominerals Identification

4.1.1. Calcium Oxalate

The differences between the monohydrate (whewellite, Wh) and dihydrate (weddellite, W) spectra of calcium oxalate have been documented by Conti et al. [32] and Petit et al. [33]. These authors point out that in the infrared spectrum, the calcium oxalate monohydrate (Wh) is characterized in the elongation zone of water molecules (3000–3600 cm^{-1}) with several peaks at 3058, 3258, 3336, 3429 and 3483 cm^{-1}. Furthermore, the pattern of calcium oxalate dihydrate has a more intense peak close

to 3469 cm^{-1}. In the studied species, there was an intense peak that varies from 3466 to 3327 cm^{-1} (Figure 1A,C,E,G,I). Other characteristic vibrations of calcium oxalate dihydrate are a weak signal at 1475 and 915 cm^{-1} that belongs to the symmetric vibrations of CO and CO + H_2O, respectively [33], and were present from 1476 to 1466 and 913 to 910 cm^{-1} (Figure 1B,D,F,H,J) in most tissues of the species studied. In the species studied, calcium dihydrate vibrations ranged from 774 to 762 cm^{-1}, very close to the reported vibrations (770 cm^{-1}), while the calcium oxalate monohydrate is assigned to 782 cm^{-1} [33]. Based on these results, we consider that calcium oxalate dihydrate is the dominant biomineral in the studied species and is mainly distributed in the three tissues. Hartl et al. [12] documented the presence of this state of hydration for other species of *Ariocarpus* (W), *Astrophytum* (W), *Echinocactus* (W) and *Mammillaria* (Wh or W). *Mammillaria* is the largest genus of the Cacteae tribe with more than 100 species; to date, only six have been studied, Wh (3) and W (3) (12, 25), plus the two here reported. The study of other *Mammillaria* species is needed to understand the variability of calcium oxalate in terms of the state of hydration as well as the identification of other elements.

4.1.2. Silica–Amorphous Hydrated Silica

Zancajo et al. [34] and Corrales-Ureña et al. [35] identified the vibration of the Si-O-Si bonds at 1090 and 1020 cm^{-1}, in amorphous silica bodies (phytoliths) from *Sorghum* and *Ananas comosus*. In *Echinocactus texensis*, amorphous silica bodies were found in the EH spectrum region, with the vibration of the Si-O-Si bond at 1014 cm^{-1} (Figure 2D). These silica bodies were distinctive in the anatomical sections of the hypodermis (Figure 3E,F). Anatomically, silica bodies were described and characterized from the visualization of stem sections [20,21,36]. In their chemical composition, just one previous study analyzed with Raman spectroscopy the presence of amorphous silica bodies in three *Opuntia* species and *Stenocereus thurberi* (Engelm.) Buxb. [36] and identified differences in their structural composition, mainly in the SiH bonds. Therefore, with Raman spectroscopy, the structure of the phytoliths could be analyzed in future studies. We consider that these amorphous silica bodies are the product of controlled biomineralization [36,37] and should be considered as a taxonomic character.

The EDS analysis supports the presence of Si in the hypodermis of *Echinocactus texensis* with the highest concentration, while the concentrations of Ca and Mg were lower. Although the precipitation phases of hypodermic biominerals were not studied in *Echinocactus texensis*, Si and Mg may be the first phase of biomineral precipitation along with some form of calcium carbonate or amorphous calcium oxalate (both have carbon, oxygen, and calcium), as in *Ficus microcarpa* L.f and *Morus alba* L. cystoliths. In both Moraceae, Si and Mg precipitate in the first phase of biomineral development, and amorphous calcium carbonate is deposited later [38]. Biominerals of *Echinocactus texensis* precipitate in cells with a small lumen (20 µm on average) compared to *Ficus* idioblasts that exceed 100 µm [38]. Density was not quantified in *Echinocactus texensis* but they are quite abundant in hypodermis strata. For these reasons, we consider that the silica bodies differ from the cystoliths and the calcium carbonate does not precipitate.

4.1.3. Calcium Carbonate

The pith of *Ariocarpus retusus* subsp. *trigonus* presented weak peaks belonging to calcium carbonate as reported by Palacio et al. [39] for some gypsophilic plants. Monje and Baran [40] identified on stems of another cactus, *Cylindropuntia kleiniae* (DC.) F.M. Knuth, vibration in the infrared between 1415 and 1422 cm^{-1}; they were assigned to the carbonate antisymmetric stretching mode of calcite. Anatomical techniques allow the identification of biominerals in certain plant tissues, however, during fixation with substances such as acetic acid, some calcium salts and phosphates could be lost [41–43]. This may be the case detected here in the pith of *Ariocarpus retusus* subsp. *trigonus*, since no previous report of calcium carbonate for any member of Cacteae is known. Probably calcium carbonate is rare in the group because they were not detected in the other species studied, even when the same method to separate biominerals were applied.

4.1.4. Unknown Biominerals

In *Astrophytum asterias*, the spectra in the EH region showed a very broad peak in the 1027 cm^{-1} region, which unlike the biominerals of *Echinocactus texensis*, they showed birefringence and were named here as prismatic crystals (see 4.1.1). However, in *Astrophytum asterias*, there was a high intensity peak in the vascular cylinder at 1028 cm^{-1} and an intense peak at 1026 cm^{-1} in the pith. These three peaks in *Astrophytum asterias* suggest a different biomineral composition, which according to Palacio et al. [39], the spectrum of the regions that presents the strongest link patterns could be assigned to some types of silicates (1100–950 cm^{-1}) or phosphates (1100–1000 cm^{-1}). We consider that these vibrations belong to silicates, probably aluminosilicates due to the presence of silicon and aluminum in biominerals detected by EDS in the hypodermis or aluminum oxides in the cortex (Figure 5). To support this finding, new FTIR spectra at 400–100 cm^{-1} are needed [44]. It is important to mention that these aluminosilicate-weddellite prismatic crystals appear to be conservative for the genus since they have been observed in the other four *Astrophytum* species studied by EDS [45]. However, they were not detected by EDS in the other stem tissues as FTIR did here for *Astrophytum asterias*.

Here, we report for the first time the presence of silicates in *Mammillaria* biominerals. In *Mammillaria melanocentra* subsp. *rubrograndis*, the peaks assigned to silicates occurred in the vascular cylinder and pith. It should be noted that these biominerals were also birefringent. Peaks assigned to silicates were also present in three of the four *Mammillaria sphaerica* tissues (Figure 2). The surprising results were the peaks in the epidermis-hypodermis of *M. sphaerica* because no vacuolar biominerals were detected in this region by microscopy. Furthermore, no biominerals other than calcium oxalate have been described for the genus [12,25]. Our results suggest that other *Mammillaria* species should be studied as mentioned above to confirm biomineral diversity.

Magnesium was detected by EDS spectra (Figure 5) but not with FTIR (Figure 2). The characteristic peaks assigned to magnesium oxalate reported by Monje and Baran [17] for other cacti such as *Opuntia* were not detected in our study by FTIR but Mg is present in traces.

4.2. Possible Functions of Biominerals in Different Tissues

Different ecological functions are attributed to biominerals in plant families [37]. Pierantoni et al. [46] showed in *Abelmoschus esculentus* that the calcium oxalates can scatter light through photosynthetic tissue and the amorphous silica bodies have a protective effect against UV radiation. The occurrence of biominerals in these species that grow in the Chihuahuan desert could be a mechanism for protecting the photosynthetic tissue and against excessive solar radiation in *Astrophytum asterias* and *Echinocactus texensis*. The presence of calcium oxalates in the cortex, vascular cylinder and pith of the stem could be explained as calcium deposits in the cellular vacuoles within the tissues, as suggested by Volk et al. [47] for *Pistia stratiotes*. The crystalline structure of calcium oxalate dihydrate has zeolitic channels that allow the adsorption of large quantities of water molecules that can diffuse "freely" in the structure [33], suggesting that these biominerals function as small water reserves. This water would be available together with the water stored in the vacuoles of cortical and pith cells, allowing plants to withstand the periods of greatest drought.

On the other hand, silicates in plants may have a role of improving the aluminum tolerance capacity, so the presence of silicon transporters shows that the deposition of phytoliths is an active and regulated process by the plant [36]. Further to this, the presence of phytoliths in plant tissues works as a defensive method against herbivores by abrasion of the teeth and reduction in the absorption of nitrogen during digestion [48], so it is possible that in cacti, the presence of silicates works in this way. These silicates were detected in experiments with *Sorghum bicolor* [49] and four cacti species [36]. In *Astrophytum asterias* and *Mammillaria melanocentra* subsp. *rubograndis*, these silicates could be present in the soil; however, the metabolic uptake capacity of silicon in the soil depends on the species. Silicon accumulation in different species could be related to the presence of silicon transporters (Lsi proteins), belonging to the Nod26-like major protein (NIP) in the plasma membranes of root

cells [4,48]. In Cacteae, the occurrence of these transporters has never been evaluated and future studies are needed.

5. Conclusions

There were vibrations associated with calcium carbonate in the P of *Ariocarpus retusus* subsp. *trigonus*. The calcium carbonate reported here increases the diversity of biominerals in cactus. The hydration state of calcium oxalate is conserved in the different tissues that were studied in the stems of the Cacteae species. Both calcium oxalate and silica bodies were present in the same species but in different tissues for *Echinocactus texensis*. The presence of silicate peaks belonging to species such as *Astrophytum asterias* and *Mammillaria sphaerica* opens the opportunity to study the role of silicates in the physiology of Cacteae species.

Supplementary Materials: The following are available online at http://www.mdpi.com/2073-4352/10/6/432/s1, Table S1. Assignment of FTIR absorption bands of biominerals extracted from tissues of Cacteae species.

Author Contributions: T.T. and A.D.l.R.-T. designed the work, T.T. collected the plants, A.D.l.R.-T. and A.M. performed the lab work and prepared the figures, A.D.l.R.-T., T.T. and A.M. analyzed the data, A.D.l.R.-T. wrote the original draft. All authors reviewed and edited the manuscript. All authors have read and agreed to the published version of the manuscript.

Funding: Funding for this research was provided by Programa de Apoyo a Proyectos de Investigación e Innovación Tecnológica, Universidad Nacional Autónoma de México (PAPIIT-UNAM); grant no. IN205419 to TT and Consejo Nacional de Ciencia y Tecnología (CONACyT), grant no. 703332 to ADR-T.

Acknowledgments: ADR-T thanks Posgrado en Ciencias Biológicas (UNAM) and AM & TT thank to Rubén San Miguel-Chávez for helping us to use the FTIR.

Conflicts of Interest: The authors declare no conflict of interest.

References

1. Skinner, H.C.W. Biominerals. *Mineral. Mag.* **2005**, *69*, 621–641. [CrossRef]
2. Arnott, H.J. Studies of Calcification in Plants. In *Calcified Tissues*; Fleish, H., Blackwood, H.J.J., Owen, M., Eds.; Springer: Berlin/Heidelberg, Germany, 1966; pp. 152–157, ISBN 978-3-642-85843-7.
3. Arnott, H.J. Three Systems of Biomineralization in Plants with Comments on the Associated Organic Matrix. In *Biological Mineralization and Demineralization*; Nancollas, G.H., Ed.; Springer: Berlin, Germany, 1982; pp. 199–218, ISBN 978-3-642-68574-3.
4. Bauer, P.; Elbaum, R.; Weiss, I.M. Calcium and Silicon Mineralization in Land Plants: Transport, Structure and Function. *Plant Sci.* **2011**, *180*, 746–756. [CrossRef] [PubMed]
5. Franceschi, V.R.; Nakata, P.A. Calcium Oxalate in Plants: Formation and Function. *Annu. Rev. Plant Biol.* **2005**, *56*, 41–71. [CrossRef]
6. McNair, J.B. The Interrelation between Substances in Plants: Essential Oils and Resins, Cyanogen and Oxalate. *Am. J. Bot.* **1932**, *19*, 255–272. [CrossRef]
7. Skinner, H.C.W.; Jahren, A.H. Biomineralization. In *Treatise on Geochemistry*; Holland, D.H., Turekian, K.K., Eds.; Elsevier Sciences: Amsterdam, The Netherlands, 2003; Volume 8, pp. 1–69, ISBN 9780080437514.
8. Cheavin, W.H.S. The Crystals and Cystolites Found in Plant Cells. Part 1: Crystals. *Microscope* **1938**, *2*, 155–158.
9. Schleiden, M.J. Beiträge zur Anatomie der Cacteen. *Mem l'Acadèmie Imp des Sci St. Pétersbg* **1845**, *4*, 335–380.
10. Bárcenas-Argüello, M.L.; Gutiérrez-Castorena, M.C.-D.-C.; Terrazas, T. The Polymorphic Weddellite Crystals in Three Species of *Cephalocereus* (Cactaceae). *Micron* **2015**, *77*, 1–8. [CrossRef] [PubMed]
11. Hartl, W.P.; Barbier, B.; Klapper, H.M.; Barthlott, W. Dimorphism of Calcium Oxalate Crystals in Stem Tissues of RHIPSALIDEAE (Cactaceae)—A Contribution to the Systematics and Taxonomy of the Tribe. *Bot. Jahrb. Syst. Pflanzengesch. Pflanzengeogr.* **2003**, *124*, 287–302. [CrossRef]
12. Hartl, W.P.; Klapper, H.; Barbier, B.; Ensikat, H.J.; Dronskowski, R.; Müller, P.; Ostendorp, G.; Tye, A.; Bauer, R.; Barthlott, W. Diversity of Calcium Oxalate Crystals in Cactaceae. *Can. J. Bot.* **2007**, *85*, 501–517. [CrossRef]

13. Monje, P.V.; Baran, E.J. On the Formation of Weddellite in *Chamaecereus Silvestrii*, a Cactaceae Species from Northern Argentina. *Z. Naturforsch. C J. Biosci.* **1996**, *51*, 426–428. [CrossRef]
14. Monje, P.V.; Baran, E.J. On the Formation of Whewellite in the Cactaceae Species *Opuntia Microdasys*. *Z. Naturforsch. C J. Biosci.* **1997**, *52*, 267–269. [CrossRef]
15. Monje, P.V.; Baran, E.J. Characterization of Calcium Oxalates Generated as Biominerals in Cacti. *Plant Physiol.* **2002**, *128*, 707–713. [CrossRef] [PubMed]
16. Rivera, E.R.; Smith, B.N. Crystal Morphology and ^{13}Carbon/^{12}Carbon Composition of Solid Oxalate in Cacti. *Plant Physiol.* **1979**, *64*, 966–970. [CrossRef] [PubMed]
17. Monje, P.V.; Baran, E.J. Evidence of Formation of Glushinskite as a Biomineral in a Cactaceae Species. *Phytochemistry* **2005**, *66*, 611–614. [CrossRef] [PubMed]
18. Jones, J.G.; Bryant, V.M. Phytolith Taxonomy in Selected Species of Texas Cacti. In *Phytolith Systematics*; Springer: Boston, MA, USA, 1992; Volume 1, pp. 215–238, ISBN 9781489911575.
19. Monje, P.V.; Baran, E.J. First Evidences of the Bioaccumulation of α-Quartz in Cactaceae. *J. Plant Physiol.* **2000**, *157*, 457–460. [CrossRef]
20. Loza-Cornejo, S.; Terrazas, T. Epidermal and Hypodermal Characteristics in North American Cactoideae (Cactaceae). *J. Plant Res.* **2003**, *116*, 27–35. [CrossRef]
21. Terrazas, T.; Loza-Cornejo, S.; Arreola-Nava, H.J. Anatomía Caulinar de las Especies del Género *Stenocereus* (Cactaceae). *Acta Botánica Venez.* **2005**, *28*, 321–336.
22. Gibson, A.C.; Horak, K.E. Systematic Anatomy and Phylogeny of Mexican Columnar Cacti. *Ann. Mo. Bot. Gard.* **1978**, *65*, 999. [CrossRef]
23. De La Rosa-Tilapa, A.; Vázquez-Sánchez, M.; Terrazas, T. Stem Anatomy of *Turbinicarpus* s.l. (Cacteae, Cactaceae) and Its Contribution to Systematics. *Plant Biosyst.* **2019**, *153*, 600–609. [CrossRef]
24. Frausto-Reyes, C.; Loza-Cornejo, S.; Terrazas, T.; De La Luz Miranda-Beltrán, M.; Aparicio-Fernández, X.; López-Mací, B.M.; Morales-Martínez, S.E.; Ortiz-Morales, M. Raman Spectroscopy Study of Calcium Oxalate Extracted from Cacti Stems. *Appl. Spectrosc.* **2014**, *68*, 1260–1265. [CrossRef]
25. López-Macías, B.M.; Morales-Martínez, S.E.; Loza-Cornejo, S.; Reyes, C.F.; Terrazas, T.; Patakfalvi, R.J.; Ortiz-Morales, M.; Miranda-Beltrán, M.D.l.L. Variability and Composition of Calcium Oxalate Crystals in Embryos-Seedlings-Adult Plants of the Globose Cacti *Mammillaria Uncinata*. *Micron* **2019**, *125*, 102731. [CrossRef]
26. Ruzin, S.E. *Plant Microtechnique and Microscopy*; Oxford University Press: Oxford, UK, 1999; ISBN 0195089561.
27. Loza-Cornejo, S.; Terrazas, T. Anatomía del tallo y de la raíz de dos Especies de *Wilcoxia* Britton & Rose (Cactaceae) del Noreste de México. *Bot. Sci.* **1996**, *59*, 13–23. [CrossRef]
28. Durak, T.; Depciuch, J. Effect of Plant Sample Preparation and Measuring Methods on ATR-FTIR Spectra Results. *Environ. Exp. Bot.* **2020**, *169*, 103915. [CrossRef]
29. Stuart, B.H. *Infrared spectroscopy: Fundamentals and Applications*; ANTS (Analytical Techniques in the Sciences); John Wiley & Sons, Ltd.: Chichester, UK, 2004; ISBN 978-0-470-85428-0.
30. Mascarenhas, M.; Dighton, J.; Arbuckle, G.A. Characterization of Plant Carbohydrates and Changes in Leaf Carbohydrate Chemistry due to Chemical and Enzymatic Degradation Measured by Microscopic ATR FT-IR Spectroscopy. *Appl. Spectrosc.* **2000**, *54*, 681–686. [CrossRef]
31. Sharma, R.; Kumar, V.; Kumar, R. Distribution of Phytoliths in Plants: A Review. *Geol. Ecol. Landsc.* **2019**, *3*, 123–148. [CrossRef]
32. Conti, C.; Casati, M.; Colombo, C.; Possenti, E.; Realini, M.; Gatta, G.D.; Merlini, M.; Brambilla, L.; Zerbi, G. Synthesis of Calcium Oxalate Trihydrate: New Data by Vibrational Spectroscopy and Synchrotron X-Ray Diffraction. *Spectrochim. Acta Part AMol. Biomol. Spectrosc.* **2015**, *150*, 721–730. [CrossRef]
33. Petit, I.; Belletti, G.D.; Debroise, T.; Llansola-Portoles, M.J.; Lucas, I.T.; Leroy, C.; Bonhomme, C.; Bonhomme-Coury, L.; Bazin, D.; Daudon, M.; et al. Vibrational Signatures of Calcium Oxalate Polyhydrates. *Chem. Sel.* **2018**, *3*, 8801–8812. [CrossRef]
34. Zancajo, V.M.R.; Diehn, S.; Filiba, N.; Goobes, G.; Kneipp, J.; Elbaum, R. Spectroscopic Discrimination of *Sorghum* Silica Phytoliths. *Front. Plant Sci.* **2019**, *10*, 1571. [CrossRef]
35. Corrales-Ureña, Y.R.; Villalobos-Bermúdez, C.; Pereira, R.; Camacho, M.; Estrada, E.; Argüello-Miranda, O.; Vega-Baudrit, J.R. Biogenic Silica-Based Microparticles Obtained as a Sub-Product of the Nanocellulose Extraction Process from Pineapple Peels. *Sci. Rep.* **2018**, *8*, 1–9. [CrossRef]

36. Wright, C.R.; Waddell, E.A.; Setzer, W.N. Accumulation of Silicon in Cacti Native to the United States: Characterization of Silica Bodies and Cyclic Oligosiloxanes in *Stenocereus Thurberi*, *Opuntia Littoralis*, *Opuntia Ficus-Indica*, and *Opuntia Stricta*. *Nat. Prod. Commun.* **2014**, *9*, 873–878. [CrossRef]
37. He, H.; Veneklaas, E.J.; Kuo, J.; Lambers, H. Physiological and Ecological Significance of Biomineralization in Plants. *Trends Plant Sci.* **2014**, *19*, 166–174. [CrossRef] [PubMed]
38. Gal, A.; Hirsch, A.; Siegel, S.; Li, C.; Aichmayer, B.; Politi, Y.; Fratzl, P.; Weiner, S.; Addadi, L. Plant Cystoliths: A Complex Functional Biocomposite of Four Distinct Silica and Amorphous Calcium Carbonate Phases. *Chem. Eur. J.* **2012**, *18*, 10262–10270. [CrossRef] [PubMed]
39. Palacio, S.; Aitkenhead, M.; Escudero, A.; Montserrat-Martí, G.; Maestro, M.; Robertson, A.H.J. Gypsophile Chemistry Unveiled: Fourier Transform Infrared (FTIR) Spectroscopy Provides New Insight into Plant Adaptations to Gypsum Soils. *PLoS ONE* **2014**, *9*, e107285. [CrossRef] [PubMed]
40. Monje, P.V.; Baran, E.J. Complex Biomineralization Pattern in Cactaceae. *J. Plant Physiol.* **2004**, *161*, 121–123. [CrossRef]
41. Berg, R.H. A Calcium Oxalate-Secreting Tissue in Branchlets of the Casuarinaceae. *Protoplasma* **1994**, *183*, 29–36. [CrossRef]
42. Lersten, N.R.; Horner, H.T. Unique Calcium Oxalate "Duplex" and "Concretion" Idioblasts in Leaves of Tribe Naucleeae (Rubiaceae). *Am. J. Bot.* **2011**, *98*, 1–11. [CrossRef]
43. He, H.; Bleby, T.M.; Veneklaas, E.J.; Lambers, H.; Kuo, J. Morphologies and Elemental Compositions of Calcium Crystals in Phyllodes and Branchlets of *Acacia Robeorum* (Leguminosae: Mimosoideae). *Ann. Bot.* **2012**, *109*, 887–896. [CrossRef]
44. Vahur, S.; Teearu, A.; Peets, P.; Joosu, L.; Leito, I. ATR-FT-IR Spectral Collection of Conservation Materials in the Extended Region of 4000–80 cm^{-1}. *Anal. Bioanal. Chem.* **2016**, *408*, 3373–3379. [CrossRef]
45. De la Rosa-Tilapa, A. Structure and Composition of Biominerals in the Stem of the Cacteae Tribe (Cactaceae). Master's Thesis, National Autonomous University of Mexico, Mexico City, Mexico, 2020.
46. Pierantoni, M.; Tenne, R.; Brumfeld, V.; Kiss, V.; Oron, D.; Addadi, L.; Weiner, S. Plants and Light Manipulation: The Integrated Mineral System in Okra Leaves. *Adv. Sci.* **2017**, *4*, 1600416. [CrossRef]
47. Volk, G.M.; Lynch-Holm, V.J.; Kostman, T.A.; Goss, L.J.; Franceschi, V.R. The Role of Druse and Raphide Calcium Oxalate Crystals in Tissue Calcium Regulation in *Pistia Stratiotes* Leaves. *Plant Biol.* **2002**, *4*, 34–45. [CrossRef]
48. Nawaz, M.A.; Zakharenko, A.M.; Zemchenko, I.V.; Haider, M.S.; Ali, M.A.; Imtiaz, M.; Chung, G.; Tsatsakis, A.; Sun, S.; Golokhvast, K.S. Phytolith Formation in Plants: From Soil to Cell. *Plants* **2019**, *8*, 249. [CrossRef] [PubMed]
49. Hodson, M.J.; Sangster, A.G. The interaction between silicon and aluminium in *Sorghum bicolor* (L.) Moench: Growth analysis and x-ray microanalysis. *Ann. Bot.* **1993**, *72*, 389–400. [CrossRef]